International Journal of Energetica (IJECA)
https://www.ijeca.info
ISSN: 2543-3717 Volume 9. Issue 2. 2024 *Page 01-11*

Design and simulation of HTL-free $CuBi_2O_4$ based thin film solar cells for performance efficiency above 36%

A.T.M. Saiful Islam[1*], Basra Sultana[2*], Rima Aktar[1], Nayan Mondal[1], Chitra Sen[1], Jhumpa Ray[1], Abdullah Al Mamun[1], Md. Dulal Haque[3,4]

[1]*Department of Electrical and Electronic Engineering, Bangabandhu Sheikh Mujibur Rahman Science and Technology University, Gopalganj-8100, BANGLADESH*
[2]*Department of Electrical & Electronic Engineering, Southeast University, Dhaka, BANGLADESH*
[3]*Department of Electronics and Communication Engineering, Hajee Mohammad Danesh Science and Technology University, Dinajpur-5200, BANGLADESH*
[4]*State Key Laboratory of infrared physics, Shanghai institute of technical physics, University of Chinese Academy of Science, CHINA*

*Corresponding author E-mail: saifulslm6@gmail.com, basrasultana@gmail.com

Abstract – *The quest for efficient and sustainable energy solutions has propelled the exploration of novel materials and strategies for enhancing the performance of thin-film solar cells (TFSCs). This work presents a comprehensive investigation into the potential of $CuBi_2O_4$ based TFSCs as a viable candidate for high-efficiency photovoltaic devices. Through rigorous numerical simulation utilizing the SCAPS-1D software, this study delves into the intricate interplay of material properties, layer characteristics, and design strategies to unlock the untapped potential of $CuBi_2O_4$ based SCs. The study extensively investigates the influence of thickness, doping levels, and defect densities of each absorber on electrical properties like open-circuit voltage (V_{oc}), short-circuit current density (J_{sc}), fill factor (FF), and power conversion efficiency (PCE). The simulation results reveal a remarkable achievement, with a recorded efficiency of 36.04%, FF of 81.11%, J_{SC} of 32.15 mA/cm², and V_{OC} of 1.38 V. These findings point to the potential of thin-film SC based on $CuBi_2O_4$ as a greener and more efficient photovoltaic option. As an absorber material for next-generation SC, $CuBi_2O_4$ exhibits potential with an efficiency of 36.04%. This investigation advances $CuBi_2O_4$-based thin-film SC and provides light on sustainable energy solutions.*

Keywords: $CuBi_2O_4$, ZnS, ETL, Solar cell, SCAPS-1D.

Received: 12/10/2024 – Revised: 16/11/2024 – Accepted: 01/12/2024

I. Introduction

A huge and noticeable shift is taking place in energy production and consumption patterns across the globe as a result of the growing demand for sustainable and environmentally friendly alternatives. Solar power stands out among these options as the most promising long-term energy solution since it is dependable, safe for the environment, and sustainable [1].

Solar energy stands out as a crucial renewable resource on a global scale, offering a promising solution to address the impending energy challenges. The market of global photovoltaic (PV) devices has grown rapidly over the last decade. Thin-film solar cells (SC) represent a promising avenue within the realm of solar energy technologies. A substrate, which can be made of materials like metal, glass, or plastic, is covered with a single or several thin layers of photovoltaic material to generate second-generation SC [2]. Second-generation SC using cadmium telluride (CdTe) and copper indium gallium selenide (CIGS) has achieved 21% and 21.7% efficiency, respectively [3], [4], [5], [6]. Commercially,

This open access article is licensed under the CC BY-NC license (https://creativecommons.org/licenses/by-nc/4.0/)

thin-film SC are used in CdTe, CIGS, and amorphous thin-film silicon (a-Si, TF-Si) technologies [2], [7], [8].

It is within this context that the investigation into $CuBi_2O_4$ based thin-film solar cells gains significance. Copper Bismuth Oxide ($CuBi_2O_4$) emerges as an intriguing absorber material due to its unique combination of properties. $CuBi_2O_4$ offers not only a high degree of environmental friendliness, being composed of abundant and non-toxic elements but also the potential for exceptional energy conversion efficiency. These characteristics position $CuBi_2O_4$ as a material of interest for advancing the frontier of thin-film solar cell technology [9], [10]. Particularly p-type $CuBi_2O_4$ has garnered significant attention as a promising material for photocathodes in SC technology due to its cost-effectiveness and ease of processing [11], [12], [13]. Additionally, it exhibits a high optical absorption coefficient surpassing 10^4 cm^{-1} [9], [14] and an optimum bandgap of 1.4 - 1.8 eV [15], [16]. $CuBi_2O_4$ is nontoxic and abundantly available, making it a desirable choice for sustainable applications.

The $CuBi_2O_4$ materials have been the focus of research in the past, and a variety of heterojunction architectures have been explored. Their photocatalytic activities have been studied in several heterostructures synthesized by hydrothermal preparation and pulsed laser deposition processes, including $WO_3/CuBi_2O_4$ [12], $CeO_2/CuBi_2O_4$ [17], $SnO_2/CuBi_2O_4$ [18], $g\text{-}C_3N_4/CuBi_2O_4$ [19], $NiO/CuBi_2O_4$ [20], and $CuO/CuBi_2O_4$ [21], [22]. A high-density p-type $CuBi_2O_4$ thin film is also produced via spin-coating onto an FTO glass substrate in preparation for PV applications [23]. In recent years, theoretical studies have been performed to improve the operational potential of $CuBi_2O_4$ based SC by exploring various buffer layers and ETL. A PCE of 22.19% is reported for the structure $ITO/SrSnO_3/CuBi_2O_4$ by selecting $SrSnO_4$ as a buffer layer [24]. Another study utilized SnS_2 as a buffer layer in an $ITO/SnS_2/CuBi_2O_4$ heterostructure, attaining a PCE of 27.73% [25]. Considering the $SnO_2/CdS/CuBi_2O_4$ structure, researchers [26] found that the inclusion of SnO_2 as a window layer resulted in a PCE of 31.41%. A structure of $ITO/TiO_2/CuBiO_4$, with TiO_2 as a buffer and ITO as an ETL, was demonstrated by Kushal et al. to exhibit a PCE of 31.21%, V_{OC} of 1.36 V, J_{SC} of 25.81 mA/cm^2, and FF of 88.77% [2]. Also, the PCE for the $SnO_2/CdS/CuBi_2O_4$ structure with absorber and buffer thicknesses of 2 µm and 7 µm, accordingly, was found to be 31.8% [27]. In an optimal absorber thickness of 2µm, a heterostructure that includes $FTO/CdS/CuBi_2O_4$ obtains a PCE of 26% [11].

In the proposed cell, ZnS [28], [29], [30] is chosen as the buffer layer due to its broad bandgap, chemical stability, and sustainability, while ITO [2], [31], [32] is used owing to its outstanding conductivity, surface consistency, and process flexibility.

Although different researchers have done some efforts to enhance PCE utilizing $CuBi_2O_4$ based solar cells, there is still a great opportunity to develop PV solar cells with suitable ETL and HTL layers due to their limited conversion efficiency. It is also necessary to optimize the thickness of the different layers, defect density, and free carrier density of the $CuBi_2O_4$ based solar cell. This research paper presents an extensive evaluation of high-efficiency TFSCs using copper bismuth oxide ($CuBi_2O_4$) absorbers, indium tin oxide (ITO) as the electron transport layer (ETL), and zinc sulfide (ZnS) as the buffer layer. The SCAPS-1D simulator was utilized to analyze the $AI/ITO/ZnS/CuBi_2O_4/Ni$ heterostructure. A thorough investigation and optimization of the effect of various factors on the cell's potential are accomplished by varying parameters such as thickness and doping density of absorber, buffer and ETL thickness, interface defect density, and device temperature. The EQE and J-V outputs of the SC are studied as well to evaluate the performance of the device. This investigation underscores the efficacy of an absorber layer for TFSCs that are both cost-effective and efficient.

II. Materials and Methods

II.2. Mathematical Models and Equations

To computationally simulate the high-efficiency, environment-friendly $CuBi_2O_4$ based thin-film SC with ZnS as a buffer layer and ITO as an electron transport layer, the drift-diffusion model is utilized within the SCAPS-1D. The drift-diffusion model describes the transport and recombination of charge carriers (electrons and holes) in the semiconductor layers of the SC. The SCAPS-1D software was developed to solve fundamental equations associated with one-dimensional semiconductors. These equations encompass Poisson's Equation (1), as well as the continuity Equations (2) and (3), which pertain to electrons and holes, all while the system maintains a state of steady equilibrium.

$$\frac{d^2\psi}{dx^2} = -\frac{q}{\in}(p - n + N_d^+ - N_A^- + \frac{\rho_{def}}{q} \quad \ldots\ldots\ldots\ldots (1)$$

$$\frac{1}{q}.\frac{dJ_x}{dx} = G - R_n \quad \ldots\ldots\ldots\ldots\ldots\ldots\ldots\ldots\ldots\ldots\ldots\ldots (2)$$

$$-\frac{1}{q}.\frac{dJ_p}{dx} = G - R_p \quad \ldots\ldots\ldots\ldots\ldots\ldots\ldots\ldots\ldots\ldots\ldots\ldots (3)$$

Here, ψ represents the electrostatic potential, q corresponds to the elementary charge of an electron, ε which can be expressed as $\in = (\in_0 \in_r)$ stands for the dielectric permittivity with $\in_0$ and $\in_r$ being the permittivity of vacuum and semiconductor respectively. Additionally, p and n denote the respective free carrier concentrations for holes and electrons. N_d^+ and N_A^- indicate the ionized donor and acceptor densities, while ρ_{def} symbolizes the charge defect density. The electron and hole current densities are denoted as J_n and J_p, while G represents the generation rate, and R_n and R_p stand for the recombination rate of electrons and holes, respectively. The movement of carriers (electrons and holes) is described by Equations (4) and (5):

$$J_n = -qD_n \frac{dn}{dx} + q\mu_n \frac{d\varphi}{dx} \dots\dots\dots\dots\dots\dots\dots\dots\dots\dots (4)$$

$$J_p = -qD_p \frac{dp}{dx} - q\mu_p \frac{d\varphi}{dx} \dots\dots\dots\dots\dots\dots\dots\dots\dots\dots (5)$$

Where D_n and D_p represent the diffusion coefficients of electrons and holes, whereas μ_n and μ_p represent the electron and hole mobilities, respectively. The generation rate can also be expressed as shown in Equation (6) [33].

$$G(\lambda, x) = \varphi_0(\lambda) e^{-d(\lambda)x} \dots\dots\dots\dots\dots\dots\dots\dots\dots\dots (6)$$

Here, λ corresponds to the wavelength of the absorbed photon, while x and α represent the depth and absorption coefficient of the absorbing material. Additionally, φ_0 stands for the incident photon flux.

Figure 1 depicts the suggested structure of AI/ITO/ZnS/$CuBi_2O_4$/Ni, along with the corresponding energy band diagram. The simulation parameters for the proposed solar cells, including each photoactive layer and the interface, are shown in Tables 1 and 2, respectively.

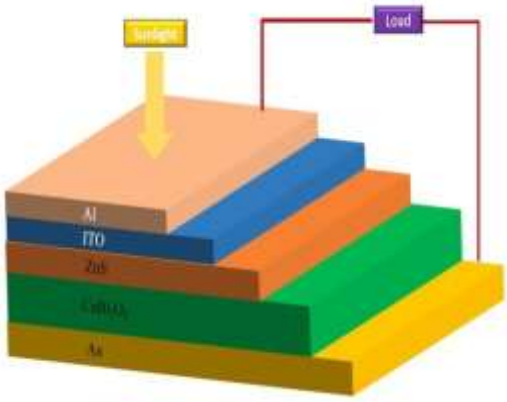

(a)

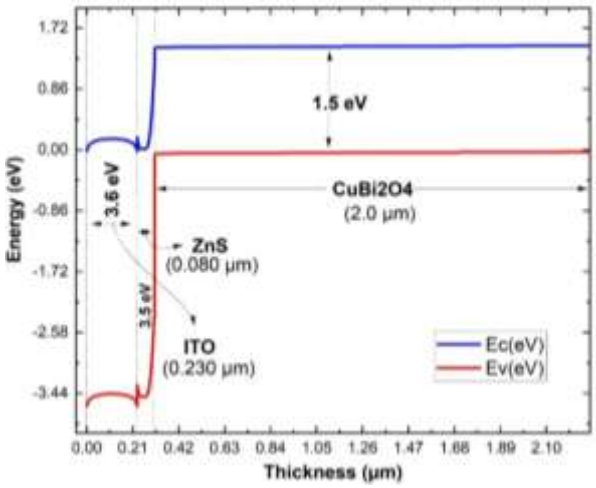

(b)

Figure 1. (a) Schematic structure and (b) band diagram of AI/ITO/ZnS/$CuBi_2O_4$/Ni solar cell

Table 1. Simulation related physical parameters of different materials at 300 K (CB = Conduction Band, VB = Valence Band)

Parameters (unit)	ITO [2], [34]	ZnS [35], [36]	$CuBi_2O_4$ [2], [11]
Thickness (μm)	0.23*	0.08*	2*
Ban gap (eV)	3.6	3.5	1.5
Electron affinity (eV)	4.1	3.9	3.72
Dielectric permittivity (relative)	10	10	34
CB effective density of states (1/cm^3)	2.20E+18	1.50E+18	1.20E+19
VB effective density of states (1/cm^3)	1.80E+20	1.70E+19	5.00E+19
Electron thermal velocity (cm/s)	1.00E+07	1.00E+07	1.00E+07
Hole thermal velocity (cm/s)	1.00E+07	1.00E+07	1.00E+07
Electron mobility (cm^2/Vs)	1.00E+02	2.50E+02	1.10E-03
Hole mobility (cm^2/Vs)	2.50E+01	7.00E+01	1.20E-03
Shallow uniform donor density (1/cm^3)	1.00E+15	1.00E+18	0
Shallow uniform acceptor density (1/cm^3)	0	0	1.70E+19*
Defect type	Acceptor	Acceptor	Donor
N_t total (1/cm^3)	1.00E+14*	1.00E+15*	1.00E+10*

N.B. * Variable parameters

Table 2. List of the interface related parameters used in this work

Parameters (unit)	ITO/ZnS	ZnS/$CuBi_2O_4$
Defect type	Neutral	Neutral
σ_e (cm^2)	1.00E-18	1.00E-19
σ_h (cm^2)	1.00E-18	1.00E-19
Characteristic energy	0.6	0.6
Total density (cm^{-2})	1.00E+10*	1.00E+10*

III. Result and discussion

III.1. *Influence of Carrier density and Thickness of $CuBi_2O_4$ Absorber Layer on Performance Parameters*

Figure 2 shows how the PV system's performance characteristics are influenced by the absorber layer thickness and the concentration of the carriers. A significant portion of incoming photons is absorbed within $CuBi_2O_4$, playing a substantial role in boosting J_{SC}. Moreover, carrier concentrations within the absorber layer exert an influence on V_{OC}. As a result, the thickness and concentration of the carriers in the photoactive layer must be optimized. In this study, the thickness and carrier concentration of the $CuBi_2O_4$ absorber layer were varied in the range of 0.1 to 2 µm and 10^{11} to 10^{20} cm^{-3}, respectively. As the $CuBi_2O_4$ absorber layer thickness increases, there is a notable enhancement in both photo-conversion efficiency and J_{SC}. Conversely, V_{OC} and FF show only minor increases with the rise in absorber layer thickness, as depicted in Figure 2. Enhanced short-wavelength photon absorption in a thicker $CuBi_2O_4$ absorber layer causes increased photo-generation of free carriers, boosting J_{SC} and efficiency [37]. When the carrier density exceeds 10^{18} cm^{-3}, the PV performance of the SC significantly improves, except the J_{SC}. With varying acceptor doping densities, the slight decrease in J_{SC} may be attributed to a higher recombination rate and a decline in charge carrier mobility [38]. As the photo-generated minority carriers encounter the depletion zone of the junction, an inherent electric field facilitates their separation [39]. Reduced acceptor density can elevate the series resistance of the device, while elevated acceptor density can lower the shunt resistance of the device, consequently diminishing the solar cell's performance [40].

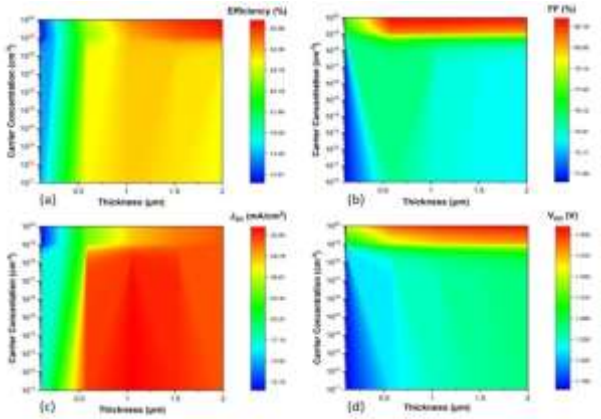

Figure 2. Influence of $CuBi_2O_4$ doping density and Thickness on Semiconductor Performance Parameters.

III.2. *Impact of Carrier Density and Thickness of ZnS Buffer Layer on Performance Parameters*

Optimizing the ZnS buffer layer is essential for attaining a high efficiency of the SC. As illustrated in Figure 3, the carrier density and thickness of the ZnS buffer layer influence a variety of SC performance parameters. In this study, the Efficiency, FF, and V_{OC} decrease with increasing buffer layer thickness and carrier concentration; conversely, J_{SC} exhibits the opposite trend. When the buffer layer is thicker and the doping concentration is higher, more photons are absorbed by the n-type buffer layer before they reach the p-type absorber. This leads to a reduction in PV parameters, as the minority carriers of the buffer layer have a shorter diffusion length, enabling a faster recombination rate [41], [42], [43]. For this structure, the buffer layer with a carrier density of 10^{18} cm^{-3} and a thickness of 0.08 µm was selected. For this carrier density and thickness, the Efficiency, FF, J_{SC}, and V_{OC} are 36.04%, 81.11%, 32.15 mA/cm^2, and 1.38 V respectively.

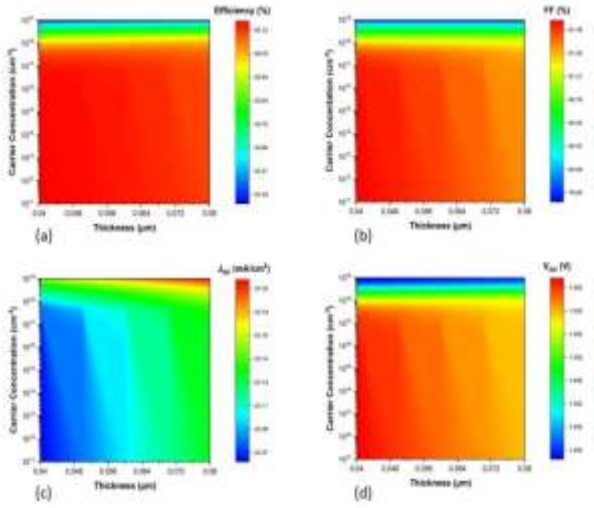

Figure 3. Influence of ZnS Carrier Density and Thickness on Semiconductor PV Parameters

III.3. *Impact of Carrier Density and Thickness of ETL as Layer on Performance Parameters*

The stability and efficacy of photovoltaic systems are significantly impacted by the electron transport layer (ETL). It facilitates the transportation of photo-generated electrons (PGEs) and holds back the opposite carriers (PGHs), thereby reducing carrier recombination velocity. By appropriately tuning the carrier concentration and thickness, the electron transport layer (ETL) can be optimized for efficient transport and collection of photo-generated carriers. The performance parameters were studied by varying the ITO thickness and carrier concentration from 0.04µm to 0.08µm and 10^{10} to 10^{18}

cm^{-3} respectively, as shown in Figure 4. Consequently, it is feasible to deduce that the thickness of the ETL has a substantial impact on the PV parameters. The PV parameters approach saturation at doping densities below 10^{16} cm^{-3}, after which it exhibits a subsequent increase [33], [40], [44]. A stronger electric field created by an increased concentration of ETL doping effectively pulls electrons and opposing minority carriers away from the ETL/buffer layer interface, reducing interface recombination [45]. The ETL facilitates adequate band alignment between the ETL and electrode, hence supporting excellent carrier collection and transportation to the electrode [33]. To achieve excellent device parameters, a layer thickness of 0.23 µm and a carrier concentration of 10^{15} cm^{-3} were utilized.

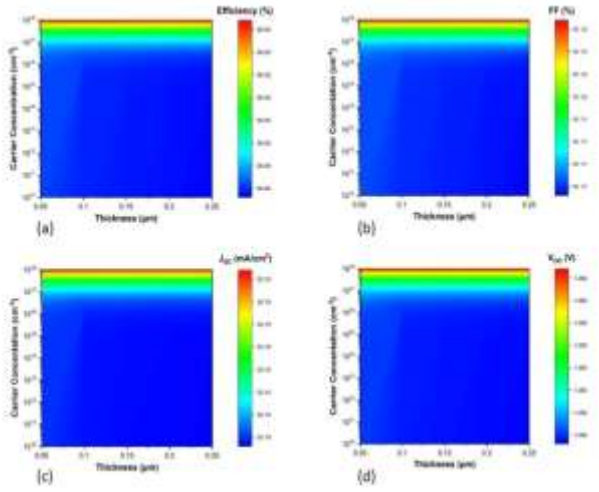

Figure 4. Influence of ETL Carrier density and Thickness on Semiconductor Performance Parameters

III.4. *Influence of Absorber Layer Defect Density*

Altering the defect density within the absorber layer and other regions of the solar cell provided insights into the relationship between defects and overall efficiency. Lower defect densities were associated with improved carrier lifetime and enhanced performance. The impact of a single donor like bulk defect density in the $CuBi_2O_4$ absorber on the cell's performance is also explored, as indicated in Figure 5.

The defect density of the $CuBi_2O_4$ layer is modified within the range of 1×10^{10} to 5×10^{15} cm^{-3}, while maintaining a constant ZnS defect density of 1×10^{15} cm^{-3}. As shown in Figure 5, V_{OC}, J_{SC}, FF, and efficiency exhibit a substantial decrease as the bulk defect density increases [46], [47], [48]. The escalation in defect states intensifies carrier recombination, thereby diminishing carrier lifetimes. The power conversion efficiencies are measured at 36.04% and 9.18% for defect densities of 1×10^{10} and 1×10^{15} cm^{-3}, respectively.

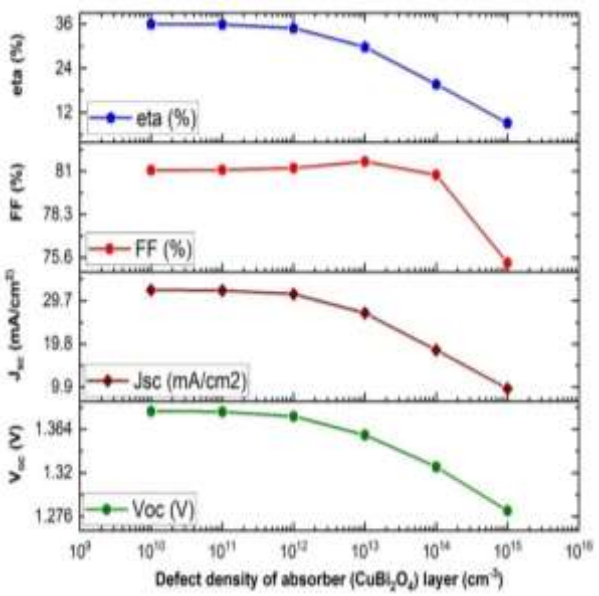

Figure 5. Effect of $CuBi_2O_4$ Absorber Defect Density on SC PV Parameters

III.5. *Dependency of Defect Density ZnS/$CuBi_2O_4$ and ITO/ZnS at the Interface on SC Performance Parameters*

The PV parameters of the SC are impacted by the existence of defect concentrations at the ZnS/$CuBi_2O_4$ and ITO/ZnS interfaces, as illustrated in Figure 6. Specifically, as the defect density changes from 10^{10} to 10^{17} cm^{-2}, the values of V_{OC}, FF, and PCE decline from 1.38 to 0.91 V, 81.11% to 78.68%, and 36.04% to 21.51%, respectively as shown in Figure 6(a). No change is observed in J_{SC} (32.15 mA/cm^{-2}) until a defect concentration of 10^{14} cm^{-2} is reached; after that, it decreases to 29.73 mA/cm^{-2}. This analysis underscores the notable influence of interface defects at ZnS/$CuBi_2O_4$, leading to a drop in the output parameters of the SC. As the defect states at the ITO/ZnS junction increase from 10^{10} to 10^{17} cm^{-2}, variations in V_{OC}, J_{SC}, FF, and Efficiency are observed as shown in Figure 6(b). A considerable quantity of carrier trap centers are created when a high concentration of defects is present at the interface, this generates in a decrease in the cell's efficiency [44], [49], [50]. Additionally, to achieve exceptional performance, the defect density at both interfaces has been maintained at 10^{10} cm^{-2}, which is consistent with the interface defect density in thin film solar cells. Additionally, to achieve exceptional performance, the defect density at both interfaces has been maintained at 10^{10} cm^{-2}, which is consistent with the interface defect density in thin film SCs.

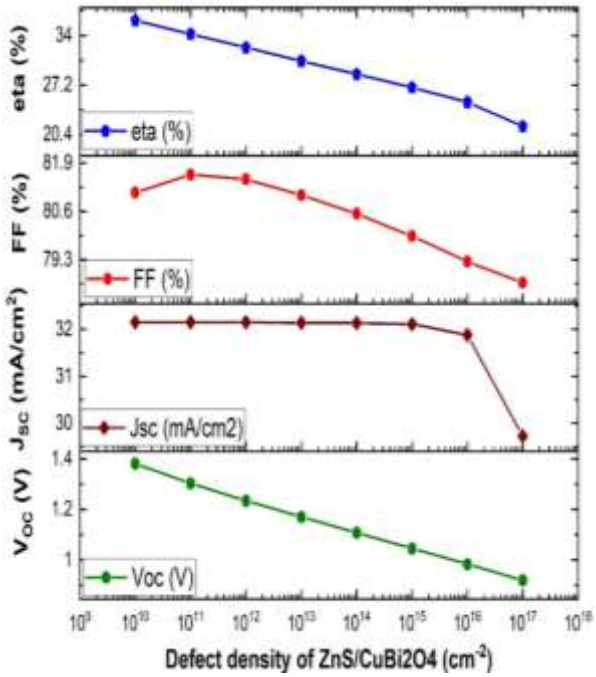

(a)

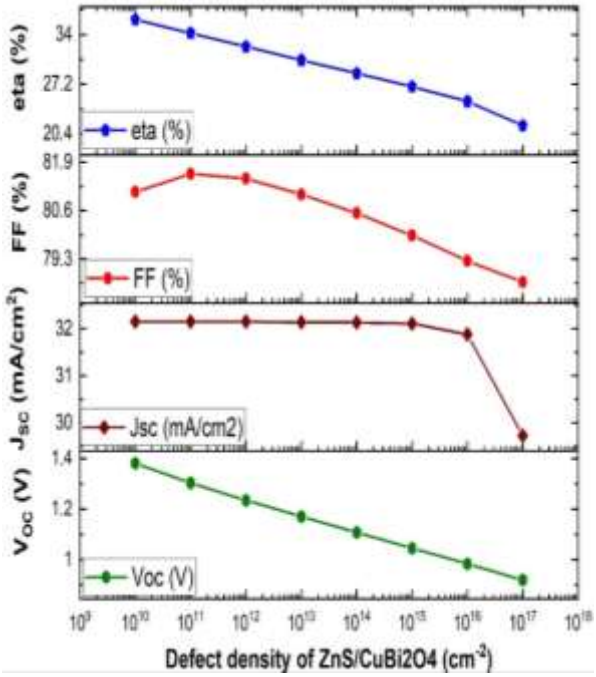

(b)

Figure 6. Effect of Defect Density at the $ZnS/CuBi_2O_4$ and ITO/ZnS Interface on Solar Cell Performance Parameters

III.6. Effect of Back Contact Metal Work Function and Temperature on SC Performance Characteristics

Figure 7 illustrates how the solar cell performance parameters respond to variations in the back contact work function and temperature. Any imperfections present at the metal-semiconductor interface can compromise solar cell efficiency by facilitating carrier recombination. The observed trend shows that V_{OC}, FF, and Efficiency experience significant enhancement as the work function increases up to 5.1 eV, after which they stabilize [46], [51], [52]. Furthermore, the J_{SC} remains relatively constant within the range delineated in Figure 7(a). When the work function is 4.7, the efficiency, V_{OC}, J_{SC}, and FF are 29.99%, 1.20 V, 32.12 mA/cm², and 77.48%, respectively. When the work function is 5.1, the corresponding values are 36.04%, 1.38 V, 32.15 mA/cm², and 81.11%. Notably, the proposed SC structure with a molybdenum (Mo) back contact attains a PCE of 31.21%, while gold (Au) achieves a PCE of 36.04%.

The PV parameters exhibit a decrease as the operating temperature rises as shown in Figure 7(b). V_{OC}'s value diminishes from 1.38 V at 300 K to 1.29 V at 450 K. This decline can be attributed to the decrease in the energy band gap of semiconductors as the temperature increases. Most semiconductors exhibit a narrowing energy band gap with rising temperatures. Consequently, the decrease in V_{OC} contributes to FF declining from 81.11% to 78.52%, while J_{SC} shifts insignificantly from 32.15 mA/cm² to 32.06 mA/cm² across the 300 to 450 K temperature range. At 300 K and 450 K, efficiencies of 36.04% and 32.53%, respectively, are estimated. This efficiency reduction, stemming from diminished V_{OC} and FF, is a result of the temperature-induced acceleration of charged particles [53]. Moreover, the rate of electron-hole recombination escalates with temperature due to lower availability of free electrons and holes [54].

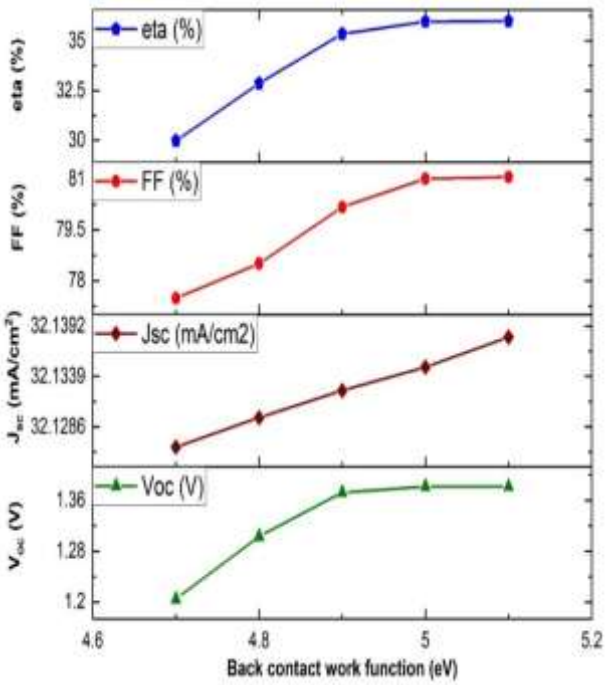

(a)

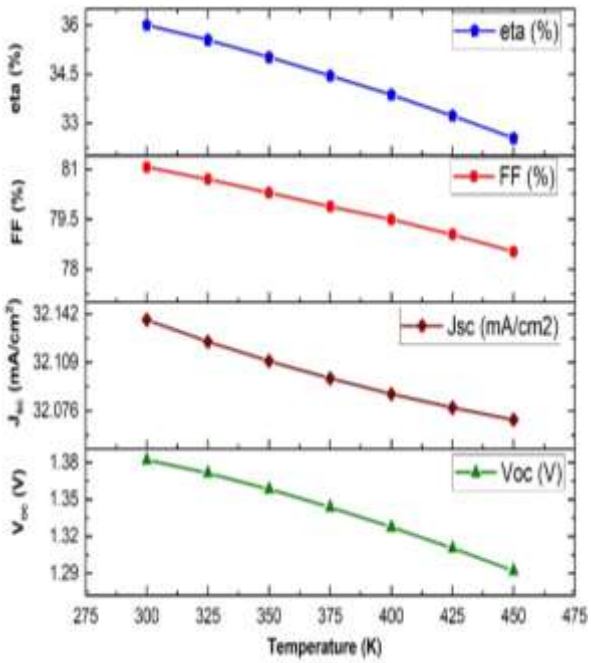

(b)

Figure 7. Effect of (a) Back Contact Metal Work Function and temperature in $CuBi_2O_4$ based Solar Cells

III.7. Influence of Series and Shunt Resistance on Cell Performance

With R_{Sh} set at 10^3 Ω-cm², the study delves into the impact of changing R_S from 0 to 5 Ω-cm² on performance in Figure 8(a). Both V_{OC} and J_{SC} remain relatively constant throughout the R_S variations. Conversely, FF and efficiency experience a notable reduction with rising R_S values. The FF and efficiency exhibit a decline from 37.80% to 33.30% and 84.94% to 75.21% respectively, as R_S increases from 0 to 5 Ω cm². Notably, the escalation of series resistance induces power losses within the solar cell, consequently leading to a decline in cell performance [46], [49]. To explore shunt resistance performance, R_{Sh} was modified within the range of 10^2 to 10^7 Ω-cm^2, while R_s was held constant at 2 Ω-cm^2. The PV parameters increase as the shunt resistance increases. As R_{Sh} increased from 10^2 to 10^7 Ω-cm^2, the efficiency enhanced by 14%. The decline in the faulty state as the device's shunt resistance increases is the reason for the increase in PV [55], [56].

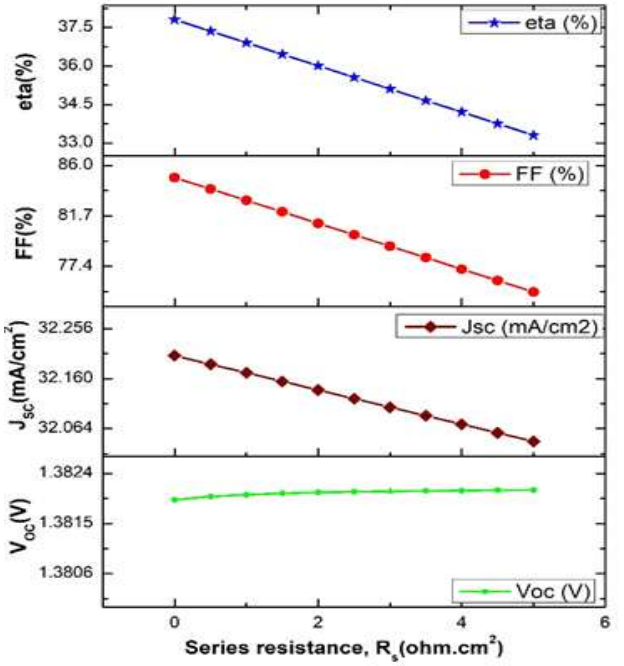

(a)

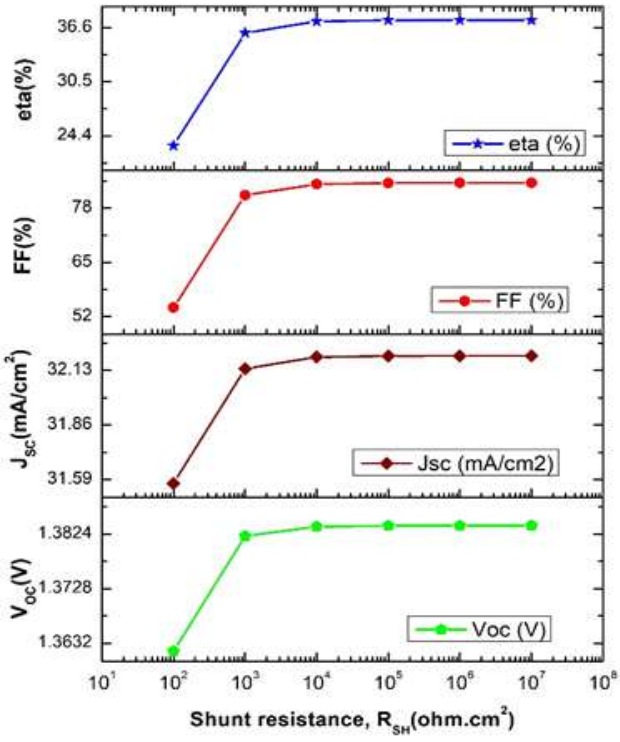

(b)

Figure 8: Effect of (a) Series Resistance and (b) Shunt Resistance on the Proposed TFSC Performance

III.8. Effect of J-V Characteristics and Quantum Efficiency

Through the manipulation of the absorber layer's $CuBi_2O_4$ thickness, Figure 9(a) illustrates the variation in J-V characteristics. Examining the J-V curve, it becomes

evident that efficiency consistently rises with an increase in absorber thickness. Figure 9(b) depicts the quantum efficiency of the $CuBi_2O_4$ based SC, illustrating its variation with changes in the absorber thickness relative to the wavelength. Notably, the quantum efficiency exhibits an increase at longer wavelengths with the growing absorber thickness, as depicted in Figure 9(b). This behavior implies heightened photon absorption through an increased absorber thickness at higher wavelengths. This phenomenon arises from the reduced generation of electron-hole pairs within the absorber layer by photons. Moreover, for longer wavelengths characterized by low energy levels, light remains unabsorbed below the band gaps, causing the quantum efficiency to diminish to zero for wavelengths beyond 830 nm.

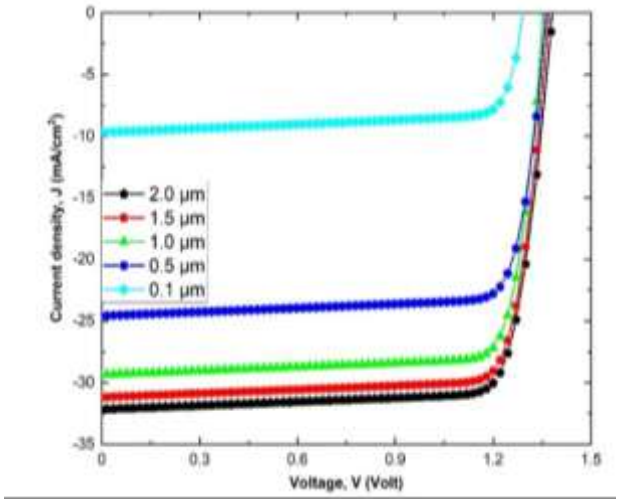

(a)

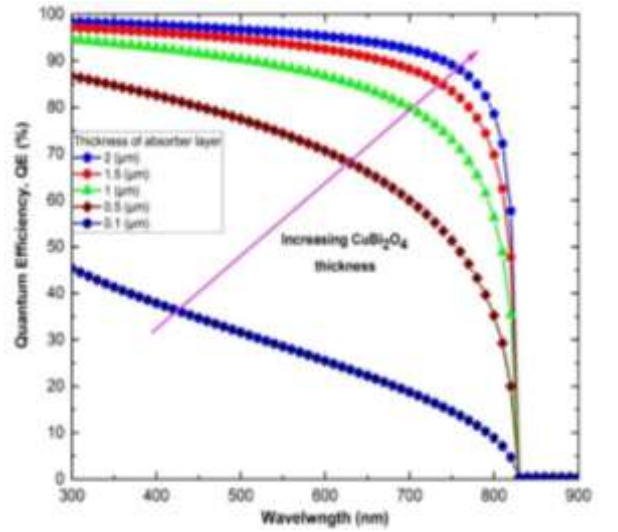

(b)

Figure 9. Influence of absorber layer's thickness on (a) J-V characteristics and (b) Quantum efficiency

III.9. Comparative study

The comparative study and outcomes of $CuBi_2O_4$ absorber SC is provided in Table 3. Previous investigations utilizing various structures reported values as high as 31.41%. There is no interface defect density introduced into the earlier work [2], [25], [26], where $CuBi_2O_4$ is used as an absorber layer, the performance is lower compared to our investigation. In contrast to prior investigations, our study achieves high J_{SC} and V_{OC}, which collectively enhance the PCE of SC. This investigation involving ITO as an ETL and ZnS as a buffer layer offers parameters and routes for making $CuBi_2O_4$ absorber SC with high efficiency of over 36% with J_{SC} of 32.15 mA/cm^2, V_{OC} of 1.38 V, and FF of 81.11%. The primary reason for the discrepancy from previous studies is the enhanced J_{SC} values generated in our proposed structure as a consequence of appropriate ETL and buffer layer selection. Having an almost perfect band gap for greatly absorbing visible spectra, the absorber material's band gap determines how much current improvement is achieved. In contrast, the value of V_{OC} is increased owing to the large built-in potential created at the absorber interface.

Table 3. Comparison of CuBi2O4 based SC with other SC

Structure	Absor. layer depth (nm)	PCE (%)	FF (%)	J_{SC} (mA/cm^2)	V_{OC} (V)	Ref
MoS_2/CZTS/CdS/ZnO	*	15.23	69.79	21.89	0.99	[57]
ZnO/CdS/CZTS	830	16.62	81.75	6.30	0.61	[58]
Al/ZnO/CdS/ZnTe/In_2Te_3 /Pt	500	20.20	91.92	10.99	2.00	[59]
ZnS/CIGS	1000	20.75	83.27	36.45	0.68	[45]
WS_2/CCZTSe/CdS/ITO	1250	26.94	83.00	44.00	0.63	[60]
ZnO/CdS/CdTe/NiO/Au	*	28.04	87.85	27.38	1.09	[61]
ITO/WS_2/$CuBi_2O_4$	*	22.84	81.3	21.08	1.33	[25]
Al/FTO/CdS/$CuBi_2O_4$/Ni	2000	26.00	84.58	31.61	0.97	[11]
Al/ITO/TiO_2/$CuBi_2O_4$/Mo	2000	31.21	87.77	25.81	1.36	[2]
SnO_2/CdS/$CuBi_2O_4$	*	31.41	85.56	25.86	1.37	[26]
Al/ITO/ZnS/$CuBi_2O_4$/Au	2000	39.39	88.41	32.21	1.38	**
Al/ITO/ZnS/$CuBi_2O_4$/Au	2000	36.04	81.11	32.15	1.38	***

N.B.
* Variable
** This work without resistance.
*** This work with resistance

IV. Conclusion

The characterization of studied sandstone revealed the presence of quartz sandstone with moderate silica content. X-ray fluorescence analyzes highlight that fraction size of 250-400 µm have a considered SiO_2 content of 89.15% recovering the other sandstone size, Associated iron oxides, aluminum oxides and other fines can reduce high application industry of this sandstone. Nonetheless, the development of enrichment techniques can apply in order to obtain the purity required. An in-depth analysis of a photovoltaic Sb_2Se_3 absorber solar cell, which utilized an ITO as an ETL and ZnS as a buffer, was carried out using the SCAPS-1D. The absorber, ETL, and buffer layer optimal parameters were determined through the study. The computation of output parameters took place using the analysis of various parameters, including operating temperature, back contact work function, series, and shunt resistance. The notable enhancement in efficiency with rising absorber thickness underscores the importance of tailoring material properties for optimized energy conversion. A potential contender for next-generation solar cell technologies, the $CuBi_2O_4$ based thin-film SC exhibits a remarkable efficiency of 36.04%. In addition to helping solar energy be used more efficiently, this high efficiency might lead to a decrease in the cost of power per unit. The observed rise in quantum efficiency at longer wavelengths with thicker absorber layers points toward the importance of maximizing photon absorption across a wide spectrum. This has implications for designing solar cells with broader spectral sensitivity, potentially enabling energy capture from a wider range of sunlight wavelengths. The outcomes of this investigation hold significant consequences for both the field of photovoltaics and the broader context of renewable energy generation.

Declaration

- The authors declare that they have no known financial or non-financial competing interests in any material discussed in this paper.
- The authors declare that this article has not been published before and is not in the process of being published in any other journal.
- The authors confirmed that the paper was free of plagiarism

Acknowledgements

To Marc Burgleman and his colleagues at the University of Electronics and Information Systems (ELIS), Department of Electronics and Information Systems, Belgium, for providing the SCAPS software package, version 3.3.07, the authors are eternally grateful.

Reference

[1] N. Singh, A. Agarwal, and M. Agarwal. Numerical simulation of highly efficient lead-free all-perovskite tandem solar cell. Sol. Energy, 2020, vol. 208, pp. 399–410

[2] K. Sarker, M. S. Sumon, M. F. Orthe, S. K. Biswas, and M. M. Ahmed. Numerical Simulation of High Efficiency Environment Friendly $CuBi_2O_4$-Based Thin-Film Solar Cell Using SCAPS-1D. Int. J. Photoenergy, 2023, vol. 2023, pp. 2–12

[3] M. Kaur and H. Singh. A review: Comparison of Silicon Solar cells and thin film solar cells. Int. J. Core Eng. Manag., 2016, vol. 3, no. 2, pp. 1–9.

[4] J. Zhao, A. Wang, and M. A. Green. 24.5% efficiency silicon PERT cells on MCZ substrates and 24.7% efficiency PERL cells on FZ substrates. Prog. Photovoltaics Res. Appl., 1999, vol. 7, no. 6, pp. 471–474

[5] M. A. Green, Y. Hishikawa, E. D. Dunlop, D. H. Levi, J. Hohl-Ebinger, and A. W. Y. Ho-Baillie. Solar cell efficiency tables (version 52). Prog. Photovoltaics Res. Appl., 2018, vol. 26, no. 7, pp. 427–436

[6] F. A. Jhuma and M. J. Rashid. Simulation study to find suitable dopants of CdS buffer layer for CZTS solar cell. J. Theor. Appl. Phys., 2020, vol. 14, no. 1, pp. 75–84

[7] Sudipta Banerjee. High Efficiency CdTe/CdS Thin Film Solar Cell. Int. J. Eng. Res., 2015, vol. V4, no. 09, pp. 700–703

[8] M. S. Islam *et al.* Defect study and modelling of SnX3-based perovskite solar cells with SCAPS-1D. Nanomaterials, 2021, vol. 11, no. 5

[9] S. P. Berglund, H. C. Lee, P. D. Núñez, A. J. Bard, and C. B. Mullins. Screening of transition and post-transition metals to incorporate into copper oxide and copper bismuth oxide for photoelectrochemical hydrogen evolution. Phys. Chem. Chem. Phys., 2013, vol. 15, no. 13, pp. 4554–4565

[10] W. Shi *et al.* Ultra-Fast Construction of Novel S-Scheme $CuBi_2O_4$/CuO Heterojunction for Selectively Photocatalytic CO_2 Conversion to CO. Nanomaterials, 2022, vol. 12, no. 18

[11] A. Hosen, M. S. Mian, and S. R. Al Ahmed. Simulating the performance of a highly efficient $CuBi_2O_4$-based thin-film solar cell. SN Appl. Sci., 2021, vol. 3, no. 5, p. 544

[12] T. Arai, Y. Konishi, Y. Iwasaki, H. Sugihara, and K.

Sayama. -Throughput Screening Using Porous Photoelectrode for the Development of Visible-. J. Comb. Chem, 2007, vol. 9, no. 4, pp. 574–581

[13] N. T. Hahn, V. C. Holmberg, B. A. Korgel, and C. B. Mullins. Electrochemical synthesis and characterization of p-$CuBi_2O_4$ thin film photocathodes. J. Phys. Chem. C, 2012, vol. 116, no. 10, pp. 6459–6466

[14] F. Wang, A. Chemseddine, F. F. Abdi, R. Van De Krol, and S. P. Berglund. Spray pyrolysis of $CuBi_2O_4$ photocathodes: Improved solution chemistry for highly homogeneous thin films. J. Mater. Chem. A, 2017, vol. 5, no. 25, pp. 12838–12847

[15] S. P. Berglund, F. F. Abdi, P. Bogdanoff, A. Chemseddine, D. Friedrich, and R. van de Krol. Comprehensive evaluation of $CuBi_2O_4$ as a photocathode material for photoelectrochemical water splitting. Chem. Mater., 2016, vol. 28, no. 12, pp. 4231–4242

[16] N. T. Hahn, V. C. Holmberg, B. A. Korgel, and C. B. Mullins. Electrochemical synthesis and characterization of p-$CuBi_2O_4$ thin film photocathodes. J. Phys. Chem. C, 2012, vol. 116, no. 10, pp. 6459–6466

[17] A. Elaziouti, N. Laouedj, A. Bekka, and R. N. Vannier. Preparation and characterization of p-n heterojunction CuBi2O4/CeO2 and its photocatalytic activities under UVA light irradiation. J. King Saud Univ. - Sci., 2015, vol. 27, no. 2, pp. 120–135

[18] E. Abdelkader, L. Nadjia, and B. Ahmed. Preparation and characterization of novel CuBi2O4/SnO2 p–n heterojunction with enhanced photocatalytic performance under UVA light irradiation. J. King Saud Univ., 2015, vol. 27, no. 1, pp. 76–91

[19] F. Guo, W. Shi, H. Wang, H. Huang, Y. Liu, and Z. Kang. Fabrication of a CuBi 2 O 4/gC 3 N 4 p–n heterojunction with enhanced visible light photocatalytic efficiency toward tetracycline degradation. Inorg. Chem. Front., 2017, vol. 4, no. 10, pp. 1714–1720

[20] J. Lee *et al.* Long-term stabilized high-density CuBi 2 O 4/NiO heterostructure thin film photocathode grown by pulsed laser deposition. Chem. Commun., 2019, vol. 55, no. 83, pp. 12447–12450

[21] S. A. Monny *et al.* Fabricating highly efficient heterostructured CuBi 2 O 4 photocathodes for unbiased water splitting. J. Mater. Chem. A, 2020, vol. 8, no. 5, pp. 2498–2504

[22] R. Gottesman *et al.* Pure CuBi2O4 photoelectrodes with increased stability by rapid thermal processing of Bi2O3/CuO grown by pulsed laser deposition. Adv. Funct. Mater., 2020, vol. 30, no. 21, p. 1910832

[23] N.-W. Kim, B.-U. Choi, H. Yu, S. Ryu, and J. Oh. Formation of high-density CuBi 2 O 4 thin film photocathodes with polyvinylpyrrolidone-metal interaction. Opt. Express, 2019, vol. 27, no. 4, pp. A171–A183

[24] V. Manjunath, Y. K. Reddy, S. Bimli, R. J. Choudhary, and R. S. Devan. 22% efficient Kusachiite solar cells of CuBi2O4 light harvester and ABO3 buffer layers: A theoretical analysis. Mater. Today Commun., 2022, vol. 32, p. 104061

[25] Y. K. Reddy, V. Manjunath, S. Bimli, and R. S. Devan. Futuristic kusachiite solar cells of CuBi2O4 absorber and metal sulfide buffer Layers: Theoretical efficiency approaching 28%. Sol. Energy, 2022, vol. 244, pp. 75–83

[26] S. E. Lachhab *et al.* Comparative evaluation of SnO2/CdS/CuBi2O4 structure performance based on SnO2 window layer numerical and experimental analysis. J. Indian Chem. Soc., 2022, vol. 99, no. 10, p. 100699

[27] S. Lachhab, A. Bliya, H. Diyagh, S. Ouhssain, E. Al Ibrahmi, and L. Dlimi. Comparative evaluation of the numerical results carried out on the buffer layer in order to optimize the performance of the SnO2/CdS/CuBi2O4 structure. Optik (Stuttg)., 2022, vol. 265, p. 169406

[28] M. N. Tousif, S. Mohammad, A. A. Ferdous, and M. A. Hoque. Investigation of Different Materials as Buffer Layer in CZTS Solar Cells Using SCAPS. J. Clean Energy Technol., Jul. 2018, vol. 6, pp. 293–296

[29] F. Qiao, K. Sun, W. Liu, Y. Xie, and H. Chu. Bandgap modulation of ZnO/ZnS heterostructures through ion exchange and their efficient transport properties. Vacuum, 2022, vol. 196, p. 110788

[30] L. Larina, D. Shin, J. H. Kim, and B. T. Ahn. Alignment of energy levels at the ZnS/Cu(In,Ga)Se 2 interface. Energy Environ. Sci., 2011, vol. 4, no. 9, pp. 3487–3493

[31] Y. Ren *et al.* The key of ITO films with high transparency and conductivity: Grain size and surface chemical composition. J. Alloys Compd., 2022, vol. 893, p. 162304

[32] R. Safa Sultana, A. N. Bahar, M. Asaduzzaman, and K. Ahmed. Numerical modeling of a CdS/CdTe photovoltaic cell based on ZnTe BSF layer with optimum thickness of absorber layer. Cogent Eng., 2017, vol. 4, no. 1, pp. 1–12

[33] M. H. Ali *et al.* Numerical analysis of FeSi2 based solar cell with PEDOT: PSS hole transport layer. Mater. Today Commun., 2023, vol. 34, p. 105387

[34] H. T. Ganem and A. N. Saleh. Enhancement of the efficiency of the CZTS/Cds/Zno/ITO Solar Cell by back reflection and buffer layers using SCAPS -1D. Iraqi J. Sci., 2021, vol. 62, no. 4, pp. 1144–1157

[35] M. B. Hosen, A. N. Bahar, M. K. Ali, and M. Asaduzzaman. Modeling and performance analysis dataset of a CIGS solar cell with ZnS buffer layer. Data Br., 2017, vol. 14, no. August, pp. 246–250

[36] K. Sobayel *et al.* Numerical modeling on prospective buffer layers for tungsten di-sulfide (WS2) solar cells by scaps-1D. Chalcogenide Lett., 2018, vol. 15, no. 6, pp. 307–315

[37] S. Fadili, B. Hartiti, A. Kotbi, A. Ridah, and P. Thevenin. Numerical simulation of solar cells besed CZTS buffer layer (ZnO1-XSX) using SCAPS-1D software. J. Fundam. Appl. Sci., 2017, vol. 9, no. 2, pp. 1001–1011

[38] S. Rai, B. K. Pandey, and D. K. Dwivedi. Designing hole conductor free tin–lead halide based all-perovskite heterojunction solar cell by numerical simulation. J. Phys. Chem. Solids, 2021, vol. 156, p. 110168

[39] X. Zhou and J. Han. Design and simulation of C2N based solar cell by SCAPS-1D software. Mater. Res. Express, 2020, vol. 7, no. 12, p. 126303

[40] K. Sarker, M. S. Sumon, M. Orthe, S. K. Biswas, and M. M. Ahmed. Numerical Simulation of High Efficiency Environment Friendly CuBi 2 O 4-Based Thin-Film Solar Cell Using SCAPS-1D. Int. J. Photoenergy, 2023, vol. 2023

[41] F. Belarbi, W. Rahal, D. Rached, and M. Adnane. A comparative study of different buffer layers for CZTS solar cell using Scaps-1D simulation program. Optik (Stuttg)., 2020, vol. 216, p. 164743

[42] T. Garmim *et al.* Effect of alternative buffer layers for SnS based solar cells: Numerical analysis using SCAPS-1D. Mater. Today Proc., 2022, vol. 66, pp. 146–150

[43] P. Chelvanathan, M. I. Hossain, and N. Amin. Performance analysis of copper–indium–gallium–diselenide (CIGS) solar cells with various buffer layers by SCAPS. Curr. Appl. Phys., 2010, vol. 10, no. 3, Supplement, pp. S387–S391

[44] A. Sunny, S. Rahman, M. Khatun, and S. R. Al Ahmed. Numerical study of high performance HTL-free CH3NH3SnI3-based perovskite solar cell by SCAPS-1D. AIP Adv., 2021, vol. 11, no. 6

[45] M. Mostefaoui, H. Mazari, S. Khelifi, A. Bouraiou, and R. Dabou. Simulation of high efficiency CIGS solar cells with SCAPS-1D software. Energy Procedia, 2015, vol. 74, pp. 736–744

[46] A. Hosen, M. S. Mian, and S. R. Al Ahmed. Simulating the performance of a highly efficient CuBi 2 O 4-based thin-film solar cell. SN Appl. Sci., 2021, vol. 3, pp. 1–13

[47] M. A. Rahman. Enhancing the photovoltaic performance of Cd-free Cu2ZnSnS4 heterojunction solar cells using SnS HTL and TiO2 ETL. Sol. Energy, 2021, vol. 215, pp. 64–76

[48] Y. Cao *et al.* Towards high efficiency inverted Sb2Se3 thin film solar cells. Sol. Energy Mater. Sol. Cells, 2019, vol. 200, p. 109945

[49] A. Hosen, S. Yeasmin, K. M. S. Bin Rahmotullah, M. F. Rahman, and S. R. Al Ahmed. Design and simulation of a highly efficient CuBi2O4 thin-film solar cell with hole transport layer. Opt. Laser Technol., 2024, vol. 169, p. 110073

[50] Y. Wang *et al.* Towards printed perovskite solar cells with cuprous oxide hole transporting layers: a theoretical design. Semicond. Sci. Technol., 2015, vol. 30, no. 5, p. 54004

[51] S. Rahman and S. R. Al Ahmed. Photovoltaic performance enhancement in CdTe thin-film heterojunction solar cell with Sb2S3 as hole transport layer. Sol. Energy, 2021, vol. 230, pp. 605–617

[52] M. N. H. Riyad, A. Sunny, M. M. Khatun, S. Rahman, and S. R. Al Ahmed. Performance evaluation of WS2 as buffer and Sb2S3 as hole transport layer in CZTS solar cell by numerical simulation. Eng. Reports, 2023, vol. 5, no. 5, p. e12600

[53] I. Alam and M. A. Ashraf. Effect of different device parameters on tin-based perovskite solar cell coupled with In2S3 electron transport layer and CuSCN and Spiro-OMeTAD alternative hole transport layers for high-efficiency performance. Energy Sources, Part A Recover. Util. Environ. Eff., 2020, pp. 1–17

[54] F. Anwar, S. Afrin, S. S. Satter, R. Mahbub, and S. M. Ullah. Simulation and performance study of nanowire CdS/CdTe solar cell. Int. J. Renew. Energy Res, 2017, vol. 7, no. 2, pp. 885–893.

[55] Naureen, Sadanand, P. Lohia, D. K. Dwivedi, and S. Ameen. A comparative study of quantum dot solar cell with two different ETLs of WS2 and IGZO using SCAPS-1D simulator., in *Solar*, MDPI, 2022, pp. 341–353.

[56] S. R. Al Ahmed, A. Sunny, and S. Rahman. Performance enhancement of Sb2Se3 solar cell using a back surface field layer: A numerical simulation approach. Sol. Energy Mater. Sol. Cells, 2021, vol. 221, p. 110919

[57] A. R. Latrous, R. Mahamdi, N. Touafek, and M. Pasquinelli. Performance Enhancement in CZTS Solar Cells by SCAPS-1D. Int. J. Thin Film. Sci. Technol., 2021, vol. 10, no. 2, pp. 7

[58] B. Drame, L. Niare, F. Yuegang, and C. Wang. Modeling of a New Solar Cell Model with ZnO/CdS Core-Shell Nanowire Arrays Embedded in a CZTS Absorber. J. Energy Technol. Policy, 2023, vol. 13, no. 1, pp. 1–14

[59] H. Ali. Improving the efficiency of ZnTe based heterojunction solar cell with In2Te3 BSF layer. 2023

[60] W. Yaseen Ali and M. Q. Kareem. Simulation of Thin-Film Solar Cells based on (CCZTSe) Using (SCAPS-1D) Program. J. Algebr. Stat., 2022, vol. 13, no. 2, pp. 902–913

[61] S. Ahmmed, A. Aktar, M. F. Rahman, J. Hossain, and A. B. M. Ismail. A numerical simulation of high efficiency CdS/CdTe based solar cell using NiO HTL and ZnO TCO. Optik (Stuttg)., 2020, vol. 223, p. 165625

.